REMARKS

Claims 1-40 are pending in this application. Reconsideration of the rejections in view of the amendments and the following remarks is respectfully requested.

Allowable Claims

Applicants gratefully acknowledge that claim 7 was merely objected to as depending from a rejected base claim, but is otherwise allowable.

The subject matter has been made into an independent form as claim 39.

Rejections under 35 USC §112, Second Paragraph

Claim 5 was rejected under 35 USC §112, second paragraph, as being indefinite because the phrase "the memory cell" lacks antecedent basis.

Accordingly, claim 5 has been amended to correct the informality.

Rejections under 35 USC §102

Claims 1, 3, 8 and 9 were rejected under 35 USC §102(e) as being anticipated by Weimer (U.S. Publication 2003/0040171).

To completely nitride up a thick silicon film, a nitriding power has to be stronger than that of ECR or ICP disclosed in Weimer. Accordingly, in the present invention, a plasma nitriding processor provided with a radial line slot antenna shown in Fig. 14 is used to generate a surface wave plasma with a high-electronic density of 1×10^{12} /cm^3 or more so that complete nitriding of the silicon film is achieved.

It is known to one skilled in the art that surface wave plasma excites and generates a strong microwave, with the use of plasma nitriding processor in Fig. 14. A document explaining this point is attached, Sugai et al., *High-density flat plasma production based on surface waves*. Weimer does not teach or suggest of generating the surface wave plasma with a high-electronic density with the use of plasma nitriding processor as in Fig. 14.

Thus, Weimer, does not teach or suggest, among other things, "a step of forming a silicon nitride film on the lower silicon oxide film to completely nitride the silicon film <u>with a surface wave plasma generated</u> by a plasma nitriding method, wherein a multilayered insulating film including at least the lower silicon oxide film and the silicon nitride film is formed," as recited in amended claim 1.

For at least this reason, claim 1 patentably distinguishes over Weimer. Claims 3, 8 and 9, depending from claim 1 also patentably distinguish over Weimer, for at least the same reason.

Thus, the 35 USC §102(b) rejection should be withdrawn.

Rejections under 35 USC §103

Claim 4 was rejected under 35 USC §103(a) as being obvious over Weimer in view of Wolf (*Silicon Processing for the VLSI Era – Vol. 2*).

As discussed above, claim 1 patentably distinguishes over Weimer. Wolf has been cited for allegedly disclosing a transistor gate insulation film comprising a multilayered oxide-nitride (ON) film, wherein the nitride layer is a charge storage film. Such disclosure, however, does not remedy the deficiency of Weimer, as discussed above.

For at least these reasons, claim 4, depending from claim 1, patentably distinguishes over

Weimer and Wolf.

Claims 1-3 and 8-11 were rejected under 35 USC §103(a) as being obvious over

Yashima (U.S. Patent No. 5,685,949) in view of Weimer.

As discussed above, claim 1 patentably distinguishes over Weimer. Yashima describes, at

the cited portion, as follows:

> As described, after the oxide film has been formed on the silicon substrate
> and then partially nitrided to form a partial nitride film in the same
> chamber, and when oxygen (O$_2$) is again used in place of nitrogen (N$_2$), it
> is possible to form an Oxide Nitride Oxide (ONO) film. The third oxide
> film may be formed by treating semiconductor wafer 1 to create an oxide
> with a depth of 40 Angstroms in 120 seconds, after the oxygen has been
> conducted into plasma treatment apparatus 10.

Thus, in Yashima, the nitride film is formed by nitriding an oxide film. Also, Yashima

merely indicates the possibility of oxidizing the particular nitride film. Yashima does not teach or

suggest "a step of forming a silicon nitride film on the lower silicon oxide film to completely

nitride the silicon film with a surface wave plasma generated by a plasma nitriding method,

wherein a multilayered insulating film including at least the lower silicon oxide film and the silicon

nitride film is formed." Thus, Yashima does not remedy the deficiencies of Weimer.

For at least these reasons, claim 1 patentably distinguishes over Weimer and Yashima.

Claims 2, 3 and 8-11, depending from claim 1 also patentably distinguish over Weimer and

Yashima, for at least the same reasons.

Claims 5 and 6 were rejected under 35 USC §103(a) as being obvious over <u>Yashima</u> in view of <u>Weimer</u>, and further in view of <u>Su et al</u> (U.S. Patent No. 6,133,096).

Claims 5 and 6 indirectly depend from claim 1. <u>Su et al</u> is cited for allegedly disclosing a method for simultaneously forming a flash memory cell and peripheral devices. Such disclosure, however, does not remedy the deficiencies of <u>Yashima</u> and <u>Weimer</u>.

For at least these reasons, claims 5 and 6, depending from claim 1, patentably distinguish over <u>Yashima</u>, <u>Weimer</u> and <u>Su et al</u>.

Thus, the 35 USC §103(a) rejections should be withdrawn.

It is submitted that nothing in the cited references, taken either alone or in combination, teaches or suggests all the features recited in each claim of the present invention. Thus all pending claims are in condition for allowance. Reconsideration of the rejections, withdrawal of the rejections and an early issue of a Notice of Allowance are earnestly solicited.

If, for any reason, it is felt that this application is not now in condition for allowance, the Examiner is requested to contact Applicant's undersigned attorney at the telephone number indicated below to arrange for an interview to expedite the disposition of this case.

In the event that this paper is not timely filed, Applicant respectfully petitions for an appropriate extension of time. The fees for such an extension or any other fees which may be due with respect to this paper, may be charged to Deposit Account No. 50-2866.

Respectfully submitted,

WESTERMAN, HATTORI, DANIELS & ADRIAN, LLP

Sadao Kinashi
Attorney for Applicant(s)
Reg. No. 48,075

Attachment: *High-density flat plasma production based on surface waves*, H. Sugai et al.

SK/sg
1250 Connecticut Ave. N.W.
Suite 700
Washington, D.C. 20036
(202) 822-1100
Q:\2003\030993\030993 amdt 1.111.doc

High-density flat plasma production based on surface waves

H Sugai, I Ghanashev and M Nagatsu

Department of Electrical Engineering, Nagoya University, Furo-cho, Chikusa-ku, Nagoya 464-8603, Japan

Abstract. Recent development of large-diameter (>30 cm) high-density (>10^{11} cm^{-3}) microwave plasma production at low pressures (<20 mTorr) without an external DC magnetic field is reviewed in view of application to the next generation ULSI devices and flat panel displays. Understanding the discharge physics—excitation, propagation and absorption of the surface wave in a flat plasma geometry under overdense conditions ($\omega_p \gg \omega$)—is indispensable for controlling the plasma. Experimental evidence of discrete surface-wave modes is clearly found in optical emission and microwave field measurements. The analysis of the full-wave electromagnetic dispersion successfully identified the observed eigenmodes. Stability analysis of the wave–plasma interaction resulted in a stability criterion predicting hysteresis loops in the power–density dependence, which were found in the experiment. A possibility of collisionless absorption of surface waves, i.e. mode conversion to electron plasma waves at the resonant layer, is discussed with the recent experimental results taken into account. From the plasma technology point of view, examples of surface-wave plasma tools (some of them commercially available) are introduced and the significance of the antenna structure is emphasized. Finally, the advantages of the surface-wave plasma source in comparison with other high-density sources are summarized.

1. Introduction

There has been a growing interest in innovative plasma sources available for manufacturing advanced electronic devices [1]. The next generation ULSI technologies require a 30 cm wafer process with 0.1 μm design rule, which needs a large-diameter (>40 cm) high-density (>10^{11} cm^{-3}) flat plasma at low pressures (<20 mTorr). Giant microelectronic devices such as flat panel displays and solar cells necessitate much larger plasmas of at least 1 m in diameter. To meet such requirements, various types of high-efficiency plasma source have been developed: electron cyclotron resonance (ECR) plasma, helicon-wave excited plasma and inductively coupled plasma (ICP). These sources are superior to a conventional capacitively coupled plasma (CCP) of low density (~10^{10} cm^{-3}) at high pressures (>100 mTorr). However, they are not always better than the CCP since high-density sources often suffer from impurities, discharge instabilities and process irreproducibility. Thus, further innovative alternative sources have been desired for the plasma processing technologies of the next generation. Here surface-wave excited plasmas are expected to be one of the most promising alternative candidates.

Surface-wave plasmas produced by microwave discharges without DC magnetic field have been exhaus-

tively investigated both theoretically and experimentally, as reviewed in [2–8]. However, almost all studies are concerned with long (sometimes extremely long [9]) plasma columns, such that the plasma diameter D is much less than the column length L. Such high-density plasma columns are clean, quiescent and reproducible, but not suitable for the recent trend of large-diameter plasma processing. Therefore some new antenna structures have been developed to obtain a large-aperture surface-wave plasma of $D>L$ [10–27]. In the present paper we give a short review of surface-wave excited flat plasma production in the absence of magnetic field, with emphasis on the slot-antenna excitation configuration we proposed recently [22–24]. Use of the slot antenna allows us to enlarge the plasma diameter very easily.

The paper is organized as follows. In the next section we briefly recall the main facts about microwave propagation in non-magnetized plasmas followed by a short review of known surface-wave plasma (SWP) tools in section 3. The subsections of section 4 present theoretical and experimental results about our slot-excited planar SWP source, including experiments in low-pressure reactive gases. In section 5 we discuss the advantages of this plasma source, and in section 6 we formulate some conclusions.
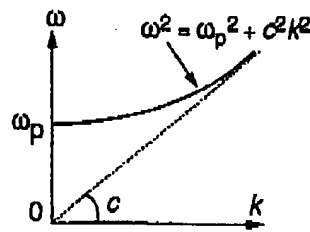
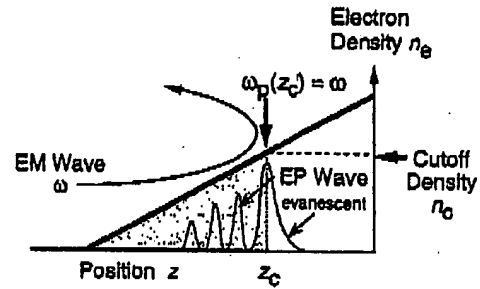Figure 1. Dispersion of plane electromagnetic waves in an infinite uniform cold collisionless plasma.

Figure 2. Electromagnetic (EM) and electron plasma (EP) wave propagation in inhomogeneous plasma.

2. Electromagnetic and electrostatic waves in non-magnetized plasmas [28, 29]

2.1. Electromagnetic waves and plasma oscillations in an infinite plasma

The dispersion equation of an electromagnetic (EM) wave propagating at a frequency of $f = \omega/2\pi$ in an infinite homogeneous non-magnetized plasma with electron density n_e is (if neglecting thermal motions and particle collisions)

$$\omega^2 = \omega_p^2 + c^2 k^2 \tag{1}$$

where k is the wave vector, c is the speed of light in free space and $\omega_p = e(n_e/\varepsilon_0 m_e)^{1/2}$ (with m_e, $(-e)$ and ε_0 being the electronic mass and charge and the permittivity of free space, respectively) is the electron plasma frequency (see figure 1). Introducing a plasma permittivity ε_p, i.e. via the phase velocity

$$v_{ph} = c/\sqrt{\varepsilon_p} = \omega/k \tag{2}$$

results in

$$\varepsilon_p = 1 - \omega_p^2/\omega^2 \tag{3}$$

which can be modified in order to take into account also the electron–neutral collision frequency for momentum transfer ν to

$$\varepsilon_p = 1 - \frac{\omega_p^2}{\omega(\omega + i\nu)}. \tag{4}$$

As in other infinite isotropic media EM waves in plasmas are transverse waves (the electric and magnetic field vectors are perpendicular to the wave vector k and to each other). For a fixed wave frequency one can define the cut-off plasma density

$$n_c = \varepsilon_0 m_e \omega^2/e^2 \tag{5}$$

for which the plasma permittivity (3) becomes zero. For example, the critical density is $n_c = 7.4 \times 10^{10}$ cm^{-3} at $\omega/2\pi = 2.45$ GHz. In the case of infinite plasmas, EM waves can propagate over longer distances with a relatively low attenuation ($|\text{Re}\,k| \gg |\text{Im}\,k|$) only at underdense conditions ($n_e < n_c$, $0 < \varepsilon_p < 1$). In overdense ($n_e > n_c$, $\varepsilon_p < 0$) plasmas EM waves are evanescent ($|\text{Re}\,k| \ll |\text{Im}\,k|$) and decay exponentially. The skin depth $\delta = 1/|\text{Im}\,k|$ derived from the dispersion equation (1) is
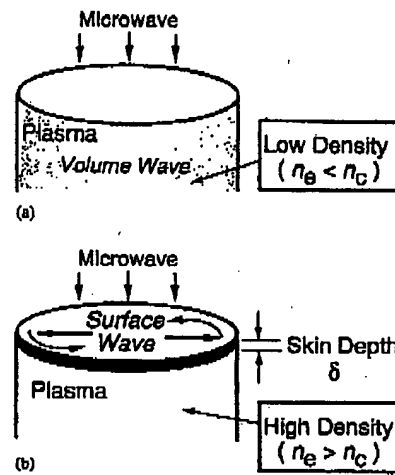
$$\delta = c/\sqrt{\omega_p^2 - \omega^2} \tag{6}$$

Figure 3. Electromagnetic wave propagation in finite (a) underdense and (b) overdense plasmas.

which becomes

$$\delta = c/\omega_p \tag{7}$$

in high density ($n_e \gg n_c$) plasmas.

If $\omega = \omega_p$ in an uniform collisionless cold plasma one should observe *plasma oscillations* with infinitely increasing amplitude (the actual amplitude will be limited by collisions, electron thermal motions and nonlinear effects). More interesting is the case of an inhomogeneous plasma with a density profile crossing the cut-off density n_0 as shown in figure 2. The wave is reflected back into the underdense region, but enters also the overdense region close to the cut-off layer, decaying exponentially there.

2.2. Electromagnetic waves in bounded plasmas

In the case of real bounded plasmas new phenomena occur. Suppose that microwaves are incident (e.g. axially) on a finite bounded plasma (e.g. cylindrical plasma column). In the low density (underdense) case (figure 3(a)) the waves penetrate into the plasma as volume waves (and give rise to volume resonances if the plasma dimensions are comparable to the wavelength determined from equation (1)). In an overdense plasma such propagation is not possible, but an electromagnetic surface wave (a wave decaying exponentially away from
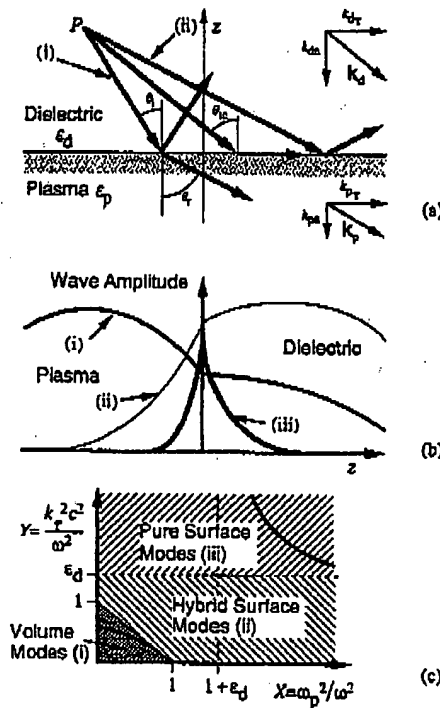
Figure 4. Electromagnetic wave propagation along a plasma–dielectric interface: (a) geometry; (b) wave field distribution on both sides of the dielectric–plasma interface for volume waves (i), hybrid surface waves (ii) and pure surface waves (iii); (c) identification of these types of wave on a (normalized) $k_\tau^2 - \omega_p^2$ diagram (the solid lines are the solutions of equation (16)).

the guiding structure [30]) can propagate along a dielectric–plasma interface (figure 3(b)), penetrating into the plasma at a few skindepths. This situation is eventually possible also along a plasma–metal boundary, because one can regard the low-density plasma sheet along the metal wall as a dielectric facing the overdense bulk plasma.

The simplest configuration capable of sustaining surface EM waves is the plane interface ($z = 0$) between a semi-infinite dielectric of permittivity ε_d and a semi-infinite plasma (see figure 4(a)). The wave vector component parallel to the surface normal is

$$k_{pn} = \sqrt{\varepsilon_p \omega^2/c^2 - k_{p\tau}^2} = \sqrt{(\omega^2 - \omega_p^2)/c^2 - k_{p\tau}^2} \qquad (8)$$

in the plasma and

$$k_{dn} = \sqrt{\varepsilon_d \omega^2/c^2 - k_{d\tau}^2} \qquad (9)$$

in the dielectric, where $k_{d\tau}$ and $k_{p\tau}$ are the wave vector components tangential to the interface in the dielectric and in the plasma, respectively. The boundary conditions along the plasma–dielectric interface require $k_{d\tau} = k_{p\tau}$, the common value being denoted hereafter simply as k_τ:

$$k_{d\tau} = k_{p\tau} = k_\tau. \qquad (10)$$

Figure 4(a) shows examples of rays of electromagnetic waves injected from the point P located in the dielectric

region with permittivity ε_d into a lower-permittivity region (plasma) of permittivity $\varepsilon_p < \varepsilon_d$ assuming that both ε_d and ε_p are real and positive (this excluding at this stage the case of overdense plasma with negative permittivity). The incidence and refraction angles with respect to the surface normal are

$$\theta_i = \tan^{-1}(k_\tau/k_{dn}) \qquad (11)$$

and

$$\theta_r = \tan^{-1}(k_\tau/k_{pn}) \qquad (12)$$

respectively. As is well known in geometrical optics, the ray trajectory follows Snell's law

$$(\varepsilon_p/\varepsilon_d)^{1/2} = \sin\theta_i/\sin\theta_r \qquad (13)$$

(this follows from (8)–(12)). It gives the critical incidence angle $\theta_{ic} = \sin^{-1}[(\varepsilon_p/\varepsilon_d)^{1/2}]$ for total reflection ($\theta_r = \pi/2$). In this situation the ray trajectories are classified into two groups as illustrated in figure 4(a), depending on the incidence angle θ_i or the value of k_τ/k_{dn}: (i) volume waves penetrating into the plasma bulk for $\theta_i < \theta_{ic}$ and (ii) volume waves totally reflected at the plasma–dielectric interface for $\theta_i > \theta_{ic}$. The amplitude of the latter decays exponentially from the interface into the low-permittivity dielectric (plasma in our case). If the plasma is overdense ε_p becomes negative and the volume waves cannot penetrate into the plasma, thus case (i) is impossible. However a new type of wave (case (iii)) occur with an amplitude decaying exponentially from the interface both in the dielectric and in the plasma. These waves are usually referred to as *surface waves*. This term is sometimes applied also to the case (ii) above. To avoid ambiguity we apply below for case (iii) the term *pure surface* or simply *surface* waves/modes, for case (ii) the term *hybrid surface* waves/modes, and to case (i) the term *volume* waves/modes.

The pure surface waves are associated with the phenomenon of total transmission (without reflection) across the interface between two semi-infinite dielectrics [30]. In the general case satisfying the boundary conditions along the interface is not possible if one takes the EM fields in both sides of the interface to be proportional to $\exp(k \cdot r)$ (of course with different values of the complex wave vector k in both media). At least in one of the media one should take a superposition of two such exponential terms (e.g. an incident *and* a reflected wave in the medium with permittivity ε_d as shown in figure 4(b)). However, taking only one exponential term in each one of the media is possible for TM (transverse magnetic) waves (waves with vanishing normal magnetic field component H_n) if [30, 24]

$$k_{pn}/\varepsilon_p = k_{dn}/\varepsilon_d. \qquad (14)$$

If k_{pn} and k_{dn} are both real this corresponds to the case of of total transmission across a dielectric interface and one can compute from (8)–(14) the (real) incidence angle

$$\theta_B = \tan^{-1}(\varepsilon_p/\varepsilon_d)^{1/2} \qquad (15)$$

which is called the *Brewster angle* [30]. Equation (14) can be fulfilled also for non-real values of k_{pn} and k_{dn}. Only the case when the imaginary parts of k_{pn} and k_{dn} have

opposite signs is physically meaningful, corresponding to wave amplitudes decaying exponentially from the interface, i.e. surface waves. A well known example are the Zenneck waves along a *lossy* dielectric (or a conductor with a finite conductivity), for which the imaginary parts of k_{pn} and k_{dn} are much less than the corresponding real parts, thus those waves are only loosely bound to the interface [30]. The fact that the permittivity (4) of an overdense weakly collisional cold plasma is negative (with a negligible imaginary part) allows equation (14) to be satisfied along a plasma-dielectric interface also for purely imaginary transverse wave numbers k_{pn} and k_{dn} (as discussed above they must have opposite signs, thus this situation is not possible along the interface between two normal lossless dielectrics with positive permittivities). Since both transverse wavenumbers are purely imaginary with k_τ real, the wave phase front is normal to the interface. Such a surface wave is very well localized in the close vicinity of the dielectric–plasma boundary. Eliminating k_{pn} and k_{dn} from (8), (9), (10) and (14) and taking into account (3) one obtains the dispersion equation of the surface waves (for the case of negligible collision freqency $\nu \ll \omega$) in the form

$$Y = \varepsilon_d \left(1 + \frac{\varepsilon_d}{X - 1 - \varepsilon_d} \right) \qquad (16)$$

where

$$X = \omega_p^2/\omega^2 \qquad Y = k_\tau^2 c^2/\omega^2.$$

As seen from equation (16), k_τ becomes infinite when

$$\omega_p/\omega = \sqrt{1 + \varepsilon_d}. \qquad (17)$$

This *surface wave resonance* sets a lower limit for the electron density at which surface-wave propagation is possible for a given wave frequency.

Figure 4 summarizes the discussion above. Depending on the sign of k_n^2 in equations (8) and (9), the wave is evanescent in the direction normal to the interface ($k_n^2 < 0$, k_n imaginary) or propagating in this direction ($k_n^2 > 0$, k_n real). Depending on whether k_n is imaginary in none, one or both media (plasma and dielectric) one can easily distinguish the three types of mode discussed above: (pure) surface modes if both k_{pn} and k_{dn} are imaginary, hybrid surface modes if k_{pn} is imaginary but k_{dn} is real and volume modes if both k_{pn} and k_{dn} are real. A sketch of the electric field distributions on both sides of the interface for these three cases is given in figure 4(b). Using equations (8) and (9) one can easily identify these modes on a (eventually normalized) ω_p^2–k_τ^2 diagram (figure 4(c)). The solutions of equation (16) are also presented in figure 4(c).

In the real finite-size plasma devices the vessel walls restrict the values of k_τ to some discrete eigenvalues allowed by the boundary conditions. For example, in the case of a rectangular vessel having metal walls at $x = \pm a/2$ and $y = \pm b/2$ a standard waveguide analysis gives the wavenumber $k_\tau = \pi \sqrt{m^2/a^2 + n^2/b^2}$ with integer m and n. The case of a cylindrical vessel is discussed below in section 4.2. Once the frequency is chosen and the value of k_τ is determined in this manner, the electron density and the perpendicular wavenumbers k_{pn} and k_{dn} are fixed from

equations (16), (8) and (9), respectively. Thus in finite-size surface-wave plasma sources the electron density values are discrete (although they may be so close to each other that the overlapping resonance courves associated with each one of them may form a continuum).

2.3. Electron plasma waves and mode conversion

In addition to the electromagnetic waves considered above, the thermal electron motion in the plasma gives rise to electrostatic waves called *electron plasma waves* (EP waves). They are longitudinal waves (the electric field vector is parallel to the wave vector k) and their dispersion equation is

$$\omega^2 = \omega_p^2 + 3v_{th}^2 k^2 \qquad (18)$$

where $v_{th} = (KT_e/m_e)^{1/2}$ (with K and T_e being Boltzmann's constant and the electron temperature, respectively) is the electron thermal velocity. In a cold plasma limit ($T_e \to 0$) this mode tends to the plasma oscillations mentioned above in section 2.1. As seen from equation (18) the EP waves can propagate only in underdense plasmas, where $\omega_p < \omega$. The dispersion curve is similar to that of the EM waves shown in figure 1. However, the phase velocity v_{ph} of the EP waves is of the order of v_{th}, while that of the EM waves is of the order of c. In surface wave sustained plasmas $v_{th} \ll c$ (T_e is a few eV), thus the wavelength (v_{ph}/f) of the EP waves should be much shorter than that of the EM waves at the same frequency $f = \omega/2\pi$. According to the dispersion equation (18) one might expect relatively long, detectable EP waves in regions with an electron density n_e slightly lower than the cut-off density n_c, e.g. on the underdense side of the cut-off transition layer in an inhomogeneous plasma.

Let us consider a nonuniform plasma whose electron density increases monotonically with the distance z as shown in figure 2. When EM waves are injected from the low-density side, and if they have an electric field along the z direction, then a linear mode conversion of the EM wave into the electrostatic EP wave takes place at the position z_c giving the cutoff density n_c where $\omega_p(z_c) = \omega$. The conversion efficiency depends on the magnitude of the density gradient and the direction of the EM wave-vector k. This type of mode conversion is well known in the field of laser–plasma interactions and the first experimental evidence using microwaves was reported by Stenzel *et al* [31]. It is accompanied by local field and absorption enhancement around z_c [32]. Recently the importance of this phenomenon (called 'resonance absorption') for surface-wave discharges is being much emphasized by some authors [33, 34]. After conversion, the EP waves propagate toward the low-density side with collisional damping. Even if the collisions are negligible, the EP waves will be easily absorbed via the Landau damping process. Therefore, the mode conversion may play a significant role in the microwave–plasma interactions in bounded plasmas.
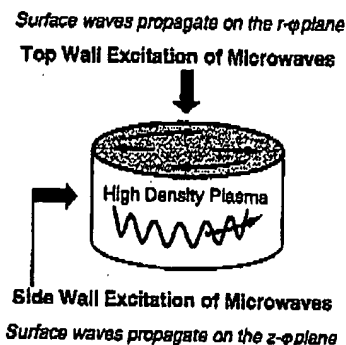
195

Surface waves propagate on the r-φ plane
Top Wall Excitation of Microwaves

High Density Plasma

Side Wall Excitation of Microwaves
Surface waves propagate on the z-φ plane

Figure 5. Approach to large-area surface-wave sustained plasmas.

3. Review of large-area surface-wave plasma tools

The most exhaustively studied case of surface waves in plasmas is that of a surface wave launched in the axial direction along a *long thin* cylindrical plasma column [2–8] (*axial excitation*). In this particular case the plasma column radius is usually comparable to or even much smaller than the skin depth δ in equation (6) so that the microwave intensity in the plasma is relatively uniform. However, surface-wave propagation is not limited to axial propagation along *long* plasma columns as demonstrated by the new surface-wave plasma sources reviewed in this section. Surface-waves can propagate, e.g. also transversely to the axis of a cylindrical plasma (and eventually sustain the plasma) if the transverse dimensions are comparable to or larger than the surface-mode wavelength. For example a cylindrical plasma could be sustained by a surface wave travelling along its flat top wall (*top wall excitation*), or along the side cylindrical wall (*side wall excitation*), or any combination thereof (see figure 5). As a result one can obtain large plasmas with the necessary geometry. Although surface-wave sustained *long* plasma columns have been usually produced by travelling waves, standing waves can also be applied, which may have some advantages, in particular improved plasma homogeneity and stronger electromagnetic fields.

Top wall excitation of surface waves seems to be the best choice for large-area flat plasma sources. The two commercially available large-area surface-wave plasma (SWP) tools (both Japanese)—the SiO₂ etcher model SW4010 by Sumitomo Metal Industries Ltd [10–12] and the resist striper model μASH8000 by Shibaura Engineering Works Co. Ltd—both apply this concept.

The SW4010 etcher has a square area of 300 mm × 300 mm (figure 6) and achieves etch rate of 0.3–0.8 μm min⁻¹ at SiO₂/Si selectivity of 5–30. The working gas is a mixture of CH₂F₂ and CF₄ at 20–30 mTorr and the applied microwave power is 1–2 kW at $f = 2.45$ GHz. This results in electron densities about 10^{12} cm⁻³. The etching rate for contact hole etching was found to be practically independent on the etch window diameter from 0.2 to 1.2 μm. A very good vertical etch profile for 1.5 μm (depth) × 0.25 μm (diameter) etch window was reported [12].

The μASH8000 resist striper has a circular area of 220 mm diameter and achieves an ashing rate of more than 4 μm min⁻¹ at a non-uniformity 5% in oxygen at 0.5 Torr (gas flow rate 1000 sccm). The applied microwave power is 1 kW at $f = 2.45$ GHz.

Other laboratory large-area plasma sources also apply the top-wall excitation concept. Tamura *et al* (Hitachi Ltd, Japan) reported [14] a circular large-area SWP source, in which the plasma is produced below a dielectric disc. The wave is launched by circular slots in the wall of a cylindrical cavity placed on top of the dielectric disc. The cavity is axially fed through a high-power coaxial cable. Recently a similar configuration has been reported by Odrobina *et al* [27]. Another (however not large-area) plasma source based also on a coaxial cavity [25] demonstrates the applicability of a large aperture coupling for top-wall excitation. The plasma is created in a chamber with an upper dielectric wall placed directly facing the open end of a coaxial-line short-circuited at the other end to form a $(5/4)\lambda$ resonator. The plasma diameter was determined by the dielectric window diameter which was close to the inner diameter of the outer coaxial line conductor (76.9 mm). Stable operation was reported down to about 0.1 mTorr at input power of 0.1–0.2 kW ($f = 2.45$ GHz), but it is not clear whether operation at such low pressures
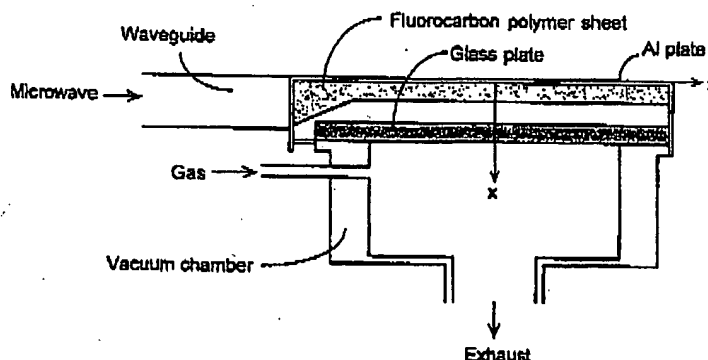

Figure 6. Schematic illustration of the SWP applicator used in the SW4010 SiO₂ etcher by Sumitomo Metal Industries, Ltd. Reproduced from Komachi K 1993 *J. Vac. Sci. Technol.* A **11** 164 by permission.

will be possible if the source is upscaled. Overdense [35] plasma was successfully created also if one put a metal sheet with many small circular apertures just below the dielectric window. This is one of the few examples, when relatively large-area non-magnetized overdense microwave plasma has been produced along a *metal* and not along a *dielectric* wall.

Another such example is provided in [26]. The source described there uses also top-wall EM wave excitation from hundreds of small slot antennas cut in a metal chamber wall facing the plasma. The slot antennas are coupled to a radial line cavity (a thin dielectric disc between two metal plates, the lower one containing the slot antennas) placed on top of the plasma chamber, which is fed at its centre by a coaxial waveguide at $f = 2.45$ or 8.30 GHz. Very good radial plasma homogeneity ($\pm 2\%$ over a diameter 300 mm area if not taking into account the last 1 cm thick region along the chamber walls) is reported. Plasma densities of the order of 10^{12} cm^{-3} have been obtained in Ar, Ar/O$_2$ and Ar/He/O$_2$ mixtures at pressures from 1 Torr down to 50 mTorr, which allowed this source to be applied for plasma oxidation of silicon wafer surfaces at relatively low (430 °C) temperature. Here again, the plasma is produced along a *metal* and not along a *dielectric* wall. A significant common feature of the above two examples of non-magnetized overdense plasma production along a *metal* wall [25, 26] is that in both cases *many* apertures *close to each other* have been used. The plasma might be sustained by a surface wave travelling along the interface between the underdense sheet along the metal wall and the overdense bulk plasma, or by the interference of the partial waves launched locally by the separate slots. The latter interpretation is possible because the distances between the slot antennas are of the same order of magnitude as the skin depth in the plasma, thus the regions excited by the separate slot antennas (each such region having a radius of a few skin depths) eventually overlap to form one big large-area plasma. In [25] and [26] there is no clear experimental evidence supporting one of these interpretations. We shall come back again to this issue in section 4.5 below.

Fujimura *et al* (Fujitsu Ltd, Japan) reported [13] a SWP tool for downflow ashing applying also top-wall irradiation of 1 kW microwave ($f = 2.45$ GHz) power through a big quartz window. The working gas was pure oxygen, or oxygen mixed with nitrogen, water vapour or hydrogen. Our slot-excited SWP source [22–26] applies also the top-wall excitation concept.

Side-wall excitation, which is already familiar from the long cylindrical plasma columns [2–8] has also been successfully applied in the design of large-area plasma sources.

Several sources of the SLAN (slot antenna) family were developed at the University of Wuppertal, Germany [15, 16]. A cross-section of one of them (SLAN I) is given in figure 7. The plasma was produced in a quartz tube of internal diameter 160 mm enclosed in a metal cylindrical chamber of larger diameter. The microwave power was fed to the chamber by many slots cut into the metal cylindrical wall. They were parallel to the cylinder axis and coupled the chamber to a rectangular waveguide wound around
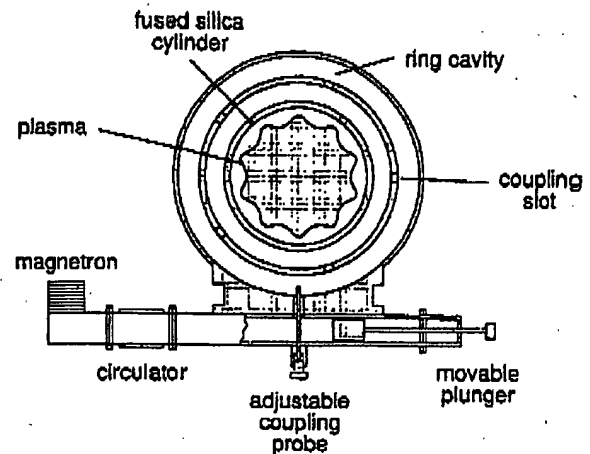

Figure 7. Cross-section of the SLAN I plasma source. Reproduced from Werner F, Korzec D and Engemann J 1994 *Plasma Souces Sci. Technol.* **3** 473. The inner quartz tube diameter is 660 mm.

it to form a ring cavity. The distance between the slots was about half a guided wavelength. The ring cavity was coupled via a single slot with an adjustable stub probe in its centre to a feeding waveguide. Additional tuning was provided by a movable plunger short-circuiting the feeding waveguide about a quarter of a guided wavelength after the coupling probe. The plasma density was about 10^{12} cm^{-3} at 1.5 kW microwave power ($f = 2.45$ GHz) in Ar at 0.08–0.8 Torr and drastically dropped at higher pressures. In the larger 660 mm 4 kW SLAN II source the density dropped from about 2×10^{11} cm^{-3} at 0.08 Torr to 10^{10} cm^{-3} at 0.8 Torr [16]. Reported plasma densities for O$_2$ were about one order of magnitude lower.

A similar approach can be found in [17], but the slots are cut not in a ring resonator but in the wall of a short-circuited waveguide bent around a glass tube of diameter 13 cm. The analysis in [17] suggests that using inclined slots results in better matching.

Another side-wall excitation SWP tool was developed in Université Paris-Sud, France [19, 20]. A high-density ($n_e = 10^{11}$–10^{12} cm^{-3} at 0.1–5 Torr) argon or oxygen plasma was sustained in a quartz tube of diameter 120 mm surrounded by a metal tube of diameter 188 mm. Microwave power of 0.2–2 kW ($f = 2.45$ GHz) was fed to the plasma by a rectangular waveguide (with its axis perpendicular to the quartz tube axis) through a single rectangular slot in the outer metal cylinder. The waveguide orientation (short cross-section side parallel to the quartz tube axis) ensured efficient coupling to the axial electric field component. This kind of surface-wave launcher is a modification of the well known surfaguide [36].

A very different approach applying much lower frequency of 149 MHz has been proposed in [21]. There a thin (a few centimetres thick) planar plasma is produced in the space between two large (130 cm × 80 cm) parallel dielectric plates. Microwave power of 0.9 kW is fed to a 10 m long Goubau transmission line (a dielectric-coated metal wire [37]) wound between the
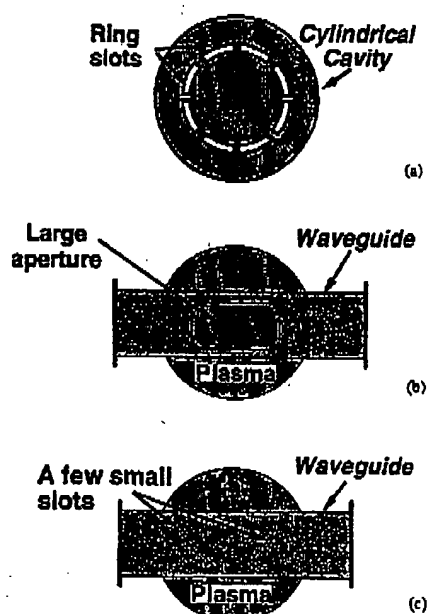
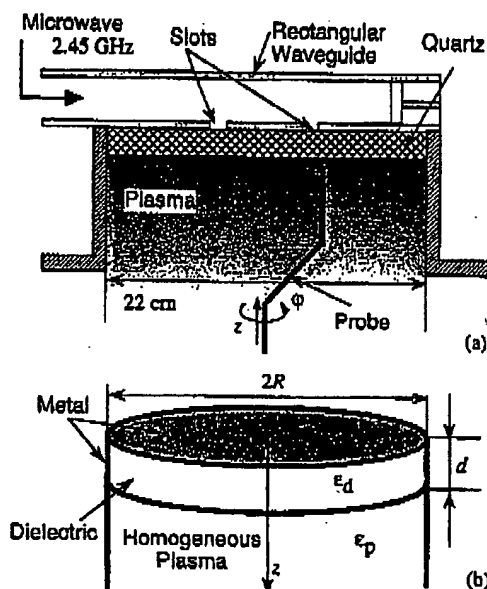Figure 8. Slot geometries for top-wall excitation.

Figure 9. Slot-antenna surface-wave planar plasma source: (a) sketch of the upper part of the source; (b) model structure for the 'two-interface model'.

dielectric plates. The surface wave propagating along the interface between the dielectric wire coating and the plasma sustains the discharge. This new plasma source stimulated theoretical and experimental research [38] of the propagation characteristics along the underlying transmission line (Goubau line immersed in an overdense plasma).

A key point in the design of any surface-wave-sustained plasma source is how the wave will be launched. The surfaguide [36] and the surfatron [39] have been successfully used for years in long thin cylindrical plasma columns. They both apply slots of some particular geometry and provide some tuning elements for better matching. Slots or larger apertures are widely used for microwave coupling to the plasma and the slot geometry and position are critical for the source performance. Some slot geometries applied in the case of SWP sources with top-wall irradiation are given in figure 8. Modifications of the ring slot geometry (figure 8(a)) have been applied as most appropriate when there is a cylindrical cavity coupled to the plasma chamber [14, 27]. Large apertures (figure 8(b)) ensure relatively good matching without additional tuning elements [10, 13, 25], but the strong coupling of the plasma to the generator may eventually cause unstable operation and poor mode selectivity. A few [22] or many [15, 26] small slots (figure 8(c)) have been also successfully used to couple the plasma to an external cavity domain (ring resonator [15], radial line cavity [26] or a waveguide operating at a high standing wave ratio [22]). The external cavity has a stabilizing effect on the source operation and produces the high electric fields necessary for the plasma ignition. Optimizing the coupling slots should be a major trend in the future development of the large-area SWP tools.

4. Measurements of surface waves and plasma performance

4.1. Experimental set-up

A sketch of the slot-excited planar circular SWP source is presented in figure 9(a) [22, 23]. The plasma is maintained at pressures 3 mTorr–1.1 Torr in a metal chamber coupled via two small slot antennas to a feeding rectangular waveguide. There is a quartz plate along the chamber wall containing the slots and the plasma is produced below this plate. The plate thickness is $d = 17$ mm and its permittivity is $\varepsilon_d = 4$. The plasma radius is $R = 11$ cm. The slots are cut in the broad wall of the feeding rectangular waveguide as shown in figure 8(c). A microwave power of 0.2–1.5 kW at $f = 2.45$ GHz is fed to the chamber. The generator is isolated from the chamber by a high-power ferrite circulator with a high-power matched load connected to its third port. An impedance transformer with remote control matches the chamber impedance to the feeding waveguide. At its other end the waveguide is short-circuited by a movable plunger. Thus a standing wave (measured standing-wave ratio about 20 dB) is maintained between this plunger and the impedance transformer. The plunger is used to optimize the chamber coupling by adjusting the standing-wave configuration to the slot antenna positions.

The plasma parameters (electron density and temperature) were measured by means of a movable Langmuir probe. The same probe was used also as antenna to measure the electric field intensity in the chamber.

4.2. Surface-wave mode identification

In order to identify the modes sustaining the plasma we refer to a simple two-interface model [24]. In this model

we simplify the chamber geometry to a vertical waveguide of an arbitrary cross-section short-circuited at its top by a metal wall (neglecting the slots). A dielectric plate of thickness d and permittivity ε_d fills entirely the upper region of the waveguide (figure 9(b)). The plasma below it is supposed to be transversely homogeneous for now (below we shall suppose axial homogeneity as well).

Such a structure can support pure transverse magnetic (TM) and transverse electric (TE) modes with $H_z = 0$ and $E_z = 0$, respectively. We experimentally found that the axial electric field component was of the same order of magnitude as the radial and azimuthal components, which excludes the case of pure TE modes, thus hereafter we consider only the TM modes. However TE modes might occur at other experimental conditions. Some details can be found in [24].

In each medium one can write down the TM-mode electric field components normal and tangential to the dielectric–plasma interface as

$$E_z(r, t) = U(\rho)\zeta(z)\,e^{-i\omega t} \qquad (19)$$

and

$$E_\tau(r, t) = \frac{1}{k_\tau^2}\nabla_\tau U(\rho)\frac{d\zeta(z)}{dz}\,e^{-i\omega t} \qquad (20)$$

respectively. In equations (19) and (20) ρ is the transverse component of the radius vector r, $\nabla_\tau = \hat{x}\frac{\partial}{\partial x} + \hat{y}\frac{\partial}{\partial y}$ is the perpendicular gradient operator and $\zeta(z)$ defines the axial field distribution ($\zeta(z)$ depends on the axial electron density profile). The scalar function $U(\rho)$ and the wave number component along the interface k_τ are found as the eigenfunctions and eigenvalues of the two-dimensional scalar Helmholtz equation $(\nabla_\tau^2 + k_\tau^2)U(\rho) = 0$ under the boundary condition for vanishing tangential electric field at the sidewalls $U = 0$. In particular, for a circular cross-section of radius R in cylindrical coordinates (ρ, φ, z) the eigenfunctions are

$$U = J_m(k_{\tau mn}\rho)\cos m\varphi \qquad m = 0, 1, 2, \ldots \qquad (21)$$

with eigenvalues

$$k_{\tau mn} = j_{mn}/R \qquad (22)$$

where j_{mn} is the nth root of the mth Bessel function $(J_m(j_{mn}) = 0)$. Substituting (21) into (19) and (20) for a circular chamber cross-section we obtain

$$E_r(r, t) = \frac{1}{k_\tau}J_m'(k_\tau\rho)(\cos m\varphi)\frac{d\zeta(z)}{dz}\,e^{-i\omega t} \qquad (23)$$

$$E_\varphi(r, t) = \frac{1}{\rho k_\tau^2}J_m(k_\tau\rho)(-m\sin m\varphi)\frac{d\zeta(z)}{dz}\,e^{-i\omega t} \qquad (24)$$

$$E_z(r, t) = J_m(k_\tau\rho)(\cos m\varphi)\zeta(z)\,e^{-i\omega t} \qquad (25)$$

thus the azimuthal distributions of E_r and E_z should have their maxima at the same azimuthal angles, while the maxima of the $E_\varphi-\varphi$ dependence should be displaced by $\Delta\varphi = \pi/2m$, which can be checked experimentally, as described below.

Figures 10(a) and (b) show the light emission patterns in the $r-\varphi$ plane observed from the bottom viewport at net absorbed power 0.4 kW in Ar at 1.05 and 0.33 Torr. The

azimuthal and radial mode numbers (m and n, respectively) of the standing mode patterns are easily identified from these pictures [40]: $m = 3$, $n = 3$ at 1.05 Torr and $m = 6$, $n = 2$ at 0.33 Torr. This identification is confirmed by the measured electric field intensity distributions. For example, figures 10(c) and (d) show the intensity of the radial microwave electric field component $\rho = 5$ cm off-axis at $z = 1$ cm from the dielectric plate plotted against the azimuthal angle φ. Bending the antenna end in the corresponding direction we measured also the dependences $|E_z|^2$ against φ and $|E_\varphi|^2$ against φ. They both were found to be similar to the $|E_r|^2-\varphi$ dependences from figures 10(c) and (d). In accordance with equations (23)–(25) the maxima of the $|E_\varphi|^2-\varphi$ dependence were found to be displaced at a half standing-wave pattern sector with respect to the maxima of the $|E_r|^2-\varphi$ and $|E_z|^2-\varphi$ dependences. All this allows us to identify the modes as transverse magnetic TM_{33} at 1.05 Torr and TM_{62} at 0.33 Torr.

The coincidence of the electric field pattern with the optical emission pattern clearly suggests the mechanism of surface-wave plasma excitation at such relatively high pressures: high-energy electrons accelerated by the strong surface-wave fields collisionally excite and ionize molecules at localized positions due to their short mean free path at high pressures. Lowering the pressure makes the optical emission pattern obscure and eventually invisible.

The measured axial electron density profile and field intensity distribution (figure 11) clearly demonstrate that the plasma was sustained by a surface wave with a skin depth of a few millimetres.

A further simplification of the two-interface model presented in figure 9(b) is to assume axial plasma homogeneity in addition to the transverse homogeneity already assumed. This results in a simple closed-form dispersion equation, which can be solved analytically (for $v = 0$) to obtain the electron plasma density ω_p (respectively the electron density n_e) at which a given mode will occur at a given wave frequency ω [24]:

$$\frac{\omega_p^2}{\omega^2} = 1 + \frac{1}{\sqrt{\omega^4/4c^4k_\tau^4 + (k_{dn}^3/\varepsilon_d^3k_\tau^2)\tan^2(k_{dn}d)} - \omega^2/2c^2k_\tau^2} \qquad (26)$$

where k_τ and k_{dn} are taken from (22) and (9), respectively. For the TM_{62} and TM_{33} modes this results (see figure 12) in electron densities of 1.4×10^{12} cm^{-3} and 2.0×10^{12} cm^{-3}, respectively, which is very close to the measured electron densities (1.3×10^{12} cm^{-3} and 2.1×10^{12} cm^{-3}) at $z = 16$ mm from the dielectric [24], thus also confirming the mode identification.

Dispersion equations for $v \neq 0$ can be found in [24] and for axially non-homogeneous plasmas in [41] and [42].

4.3. Mode jumps and stability

A typical recorded power–density dependence of the slot-excited planar SWP source is shown in figure 13 [43, 44]. The power P_{in} on the abscissa is *not* the net absorbed power, but the incident power from the microwave generator. Increasing this power *does not* generally cause an immediate response of the plasma density. The plasma
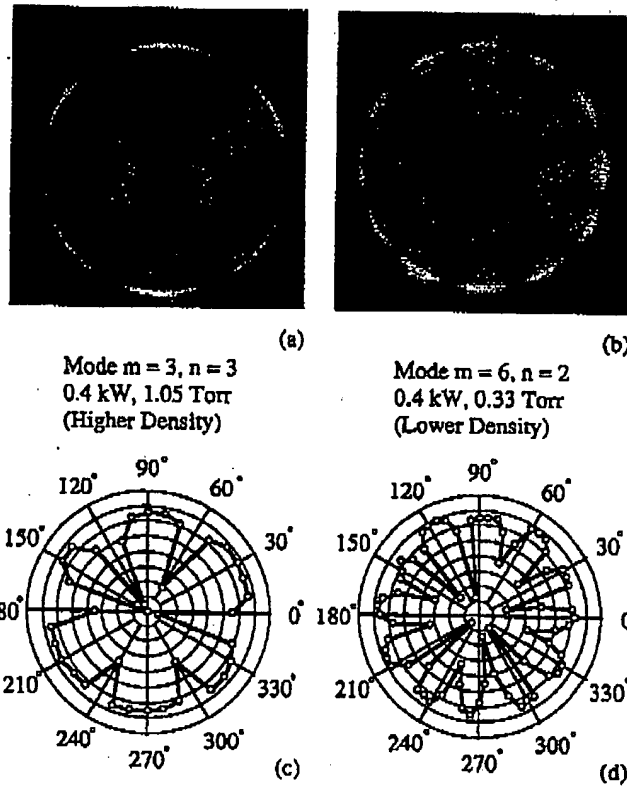
(a)   (b)

Mode m = 3, n = 3   Mode m = 6, n = 2
0.4 kW, 1.05 Torr   0.4 kW, 0.33 Torr
(Higher Density)   (Lower Density)

(c)   (d)

Figure 10. Photographs of the light emission patterns (a, b) and measured azimuthal distribution (c, d) of the microwave field intensity (radial electric field component at $p = 5$ cm, $z = 1$ cm) in Ar for net absorbed power 0.4 kW at 1.05 (a, c) and 0.33 Torr (b, d).
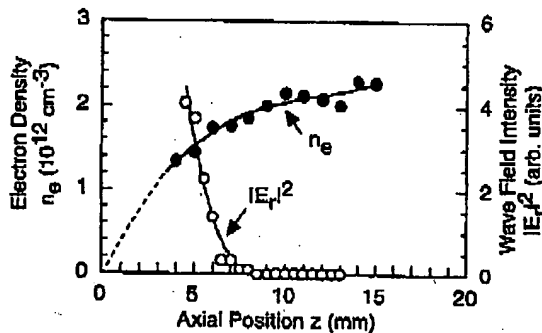

Figure 11. Axial electron density and microwave field profiles in Ar at 1.05 Torr. The net input power was 0.4 kW.

sticks to some discrete density values. This is not surprising for the present configuration. The 'preferred' density values are those values which ensure that some of the resonant eigenmodes will appear exactly at the excitation frequency (2.45 GHz in the present experiment), thus they should be approximately given by equation (26). The horizontal dashed lines in figure 13 denote the values obtained for $\omega/2\pi = 2.45$ GHz for the TM_{53}, TM_{62} and TM_{33} modes. The numbers in brackets are the azimuthal and radial mode numbers for the corresponding branch of the power-density dependence, as identified from the observed light emission pattern (for the branch denoted '(*, *)' no clear

mode pattern was observed, thus suggesting that it was a superposition of two very close eigenmodes). The coincidence of the measured and computed plasma densities is very good.

The origin of the hysteresis loops can be easily understood if we examine what determines the incident power P_{in} necessary to sustain a given average plasma density $\bar{n}_e$. It can be expressed as

$$P_{in}(\bar{n}_e) = \bar{n}_e V \Theta(\bar{n}_e)/[1 - \Gamma^2(\bar{n}_e)] \qquad (27)$$

where V is the plasma volume, Θ is the average power necessary to sustain one electron–ion pair in the discharge and Γ^2 is the power reflection coefficient of the chamber. Since Γ^2 has deep minima around the resonance densities defined by equation (26), P_{in} will also have deep minima at approximately the same resonant densities (figure 14). If P_{in} decreases with increasing density any density fluctuation will increase exponentially, thus only the rising branches of the curve defined by (27) are stable and observable. At the end of these branches a mode jump to another rising curve branch will occur [44].

Physically the plasma behaviour in the constant-density stable regions is as follows. Any increase ΔP_{in} of the incident wave power P_{in} causes a slight increase in the plasma density. This causes a (not proportional) significant increase of the chamber power reflection coefficient Γ^2, since the plasma density is shifted away from its resonant
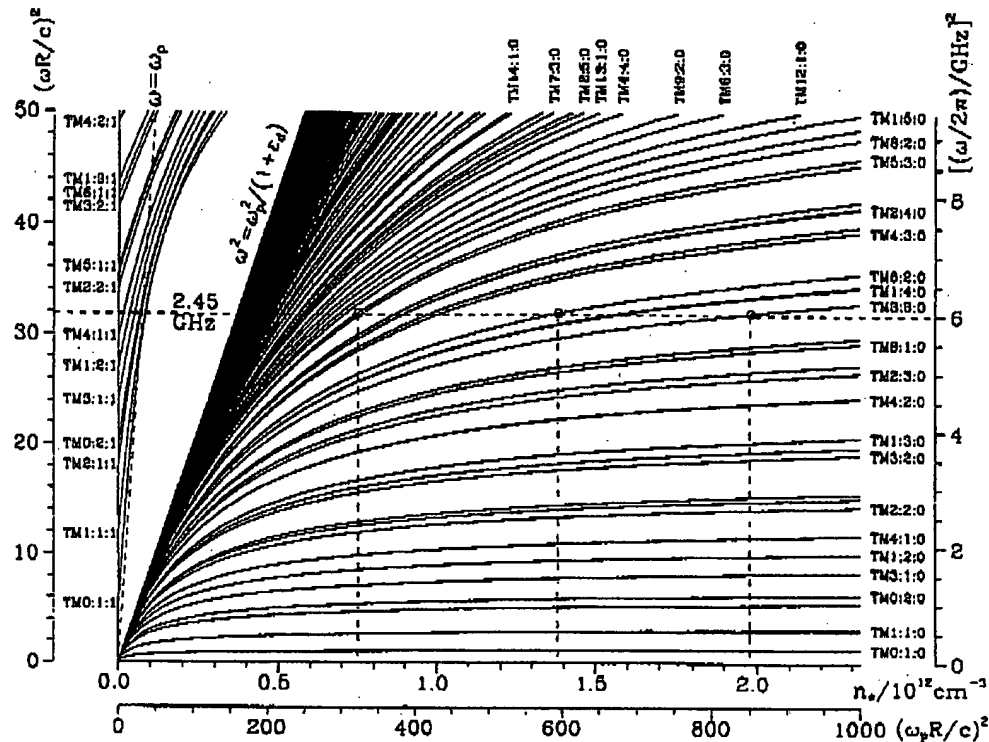
200

Figure 12. Computed resonance frequencies of the TM modes in a cylindrical chamber of radius $R = 110$ mm for $\varepsilon_d = 4$, $d = 17$ mm. Not all modes are labelled. Reproduced from [24] by permission.
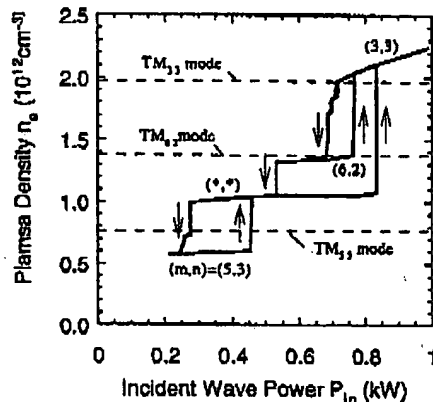

Figure 13. Density jumps and hysteresis in the slot-excited SWP source in Ar at 0.27 Torr. The plasma density was measured locally at $z = 10$ mm from the dielectric interface $\rho = 5$ cm off-axis.

value, the latter being the density that ensures best chamber matching. Thus only a small portion of the additional power ΔP_{in} enters the chamber, most of it is reflected back: the net power absorbed in the plasma remains practically the same, this being consistent with the almost constant plasma density for a given mode.

This behaviour can be successfully used to ensure stable plasma source operation. When surface-wave plasmas are operated near the critical condition for mode transition

a discontinuous density jump, which is unfavourable for plasma processing, may occur. To avoid this, it is enough to chose a relatively long and preferably high-density branch in the power–density dependence and locate the operating point not very close to the branch ends. This ensures a stable value of the plasma density not affected by the inevitable pressure or power fluctuations. Eventually it may be necessary to increase the input power for a short time in order the operating point to jump to a higher-density branch, but after the jump occurs, the power may be decreased again to a much lower value, provided this value is still far enough from the lowest power of the respective hysteresis branch. Stability will be better if only a few modes are effectively excited. Thus, it will be significant to design the positions and number of slot antennas in a way ensuring selective excitation of the proper mode(s).

4.4. Power absorption mechanism

Usually the microwave power is assumed to be transferred from the electric field E of the surface waves to the electrons in the plasma by collisional absorption. In this case the absorbed power is proportional to $[v/(\omega^2 + v^2)]E^2$. At low pressures this power absorption channel is not efficient due to the low collision frequencies. For example in Ar at 10 mTorr and 2.45 GHz $v/\omega \sim 10^{-3}$. Thus one should expect that collisionless absorption mechanisms will play an important role too. Stochastic transit-time heating [45, 46] is effective if the electron transit time
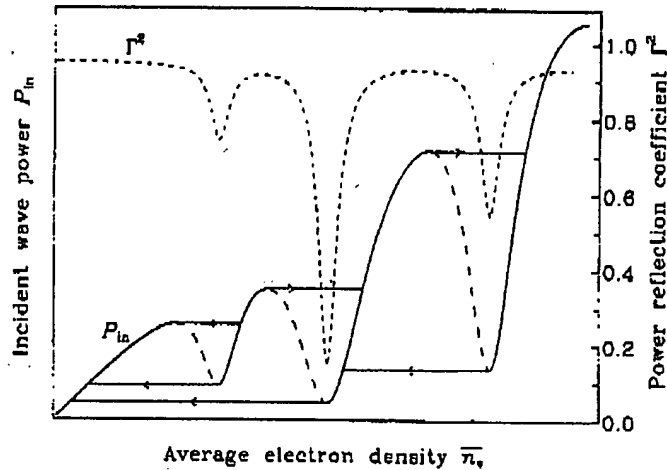
Figure 14. Sketch of typical density dependences of the power reflection coefficient Γ^2 and the necessary input power P_{in}, demonstrating the origin of the hysteresis loops. The dashed parts of the P_{in} curve correspond to the unstable states of the discharge.

Δ/v_{th} (the time for passing the strong field region of size Δ) is shorter or of the order of the wave period $2\pi/\omega$. In our case, if we take Δ to be the skin depth δ, we get $\delta/v_{th} \gg 2\pi/\omega$. Still transit-time stochastic heating may be important if one considers the existence of a sharp electric field peak of width $\Delta \ll \delta$ at the resonance surface $\omega_p = \omega$ [45,47]. Another possible power absorption channel is mode conversion from a long-wavelength electromagnetic (EM) wave to a short-wavelength electron plasma (EP) wave [31] (see section 2.3 above). It is expected to occur in the transition layer between the overdense bulk plasma and the underdense sheet along the chamber walls.

We tried to detect the existence of EP waves in the transition layer experimentally. They might be identified by the fact that they are slow waves (their phase velocity is of the order of the electron thermal speed), this resulting in a very short wavelength $\lambda_{EPW} \sim 1$ mm, much shorter than the wavelength of the electromagnetic waves.

We were not able to detect EP waves when the plasma was created in CW (continuous wave) mode. This is not surprising, taking into account the high electron density of the order 10^{12} cm^{-3} (much higher than the cut-off density $n_c = 7.4 \times 10^{10}$ cm^{-3}) in the bulk plasma. In such conditions the underdense layer along the chamber walls, where one might expect to detect the EP waves, is extremely thin.

We performed also pulsed mode experiments [48,49] with the main purpose to check how strongly the microwave field influences the Langmuir probe measurements (we found that the probe characteristics taken 2 μs before and 2 μs after the microwave was turned off were practically identical, this indicating that in our case the microwave did not affect the probe measurements). The microwave was turned on and off with a repetition frequency of 5 kHz, peak power 0.3 kW and duty ratio 60% (on time 120 μs, off time 80 μs, rise time about 0.2 μs). In the early times (the first 10–20 μs) after the microwave is turned
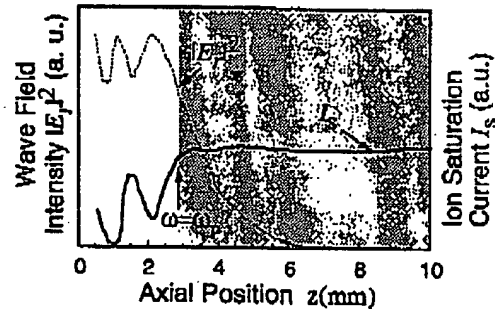

Figure 15. Recorded axial distributions of the microwave intensity and ion saturation current in pulse-modulated argon plasma at 5 μs after turn-on believed to demonstrate the occurrence of standing electron plasma waves along the transition layer.

on the plasma density is much lower than the steady state density reached later, thus the conditions for detecting the EP waves are much more favourable. We performed time-and space-resolved measurements using an axially movable antenna/Langmuir probe and a box-car integrator. We believe that figure 15 proves the existence of the EP waves. In this figure we have recorded the axial distribution of the microwave intensity at $z < 10$ mm from the dielectric window, as measured 5 μs after the microwave was turned on. In the region 0–3 mm one can clearly see a standing wave pattern with wavelength ~ 1 mm, which we believe is a standing EP wave. In the same figure we have recorded the axial distribution of the ion saturation current, which can be thought of as proportional to the electron density. It shows that the plasma density is modulated with the same wavelength as the microwave field intensity. This might be attributed to a nonlinear density depression (caviton) [50–52] caused by the strong EP wave electric field.
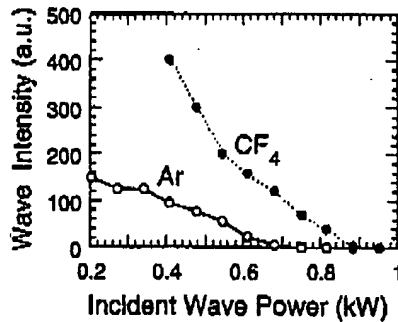
Figure 16. Power dependence of the microwave field intensity in the bulk plasma (at $z = 3$ cm from the dielectric window) in Ar (solid line) and CF_4 (dashed line) at 15 mTorr.

4.5. Operation at low pressures and in reactive gases

Both decreasing the gas pressure down to about 10 mTorr and/or replacing the noble gas (Ar) with an non-noble reactive one (CF_4) results in lower electron densities than those observed in Ar at 0.2–1 Torr. If the input power is not high enough the plasma may be underdense or only slightly overdense. This is demonstrated in figure 16, which gives the relative wave intensity in the bulk plasma (at $z = 3$ cm from the plasma–dielectric interface) as a function of the applied microwave power for Ar and CF_4 at a gas pressure of 15 mTorr. At the first glance it might be unusual that the field intensity does not increase but *decreases* with increasing the input power. However this effect can be easily explained if we take into account that (according to equation (7)) the wave skin depth δ in the plasma is shorter at higher electron densities

$$\delta \approx \text{constant} \times n_e^{-1/2} \qquad (28)$$

and that the electron density n_e is roughly proportional to the net absorbed power P

$$n_e \approx \text{constant} \times P. \qquad (29)$$

Indeed, the field intensity E at a given distance z from the plasma–dielectric interface will be roughly proportional to $P^{1/2}$ and decay exponentially as $\exp(-z/\delta)$ into the plasma:

$$E^2 \propto P \exp(-2z/\delta). \qquad (30)$$

For a constant z, taking into account (28) and (29), one can rewrite (30) as

$$E^2 \propto P \exp(-\sqrt{P/P_0}) \qquad P_0 = \text{constant} \propto z^{-2}. \qquad (31)$$

If $P > 4P_0$ this is a decreasing function of P, in accordance with what we observed experimentally. The higher microwave field intensity observed in CF_4 plasmas is due to the lower electron density, respectively longer skin depth, allowing deeper surface wave penetration into the plasma.

In the case of argon, the lowest pressure to ignite the discharge at 0.8 kW was about 15 mTorr and the plasma could be sustained down to the low pressure of about

3 mTorr. It will be possible to further decrease the working pressure by using magnetic multiple confinement.

These experimental results demonstrate the applicability of the slot-excited planar SWP source for low-pressure plasma processing in reactive gases, as already demonstrated for plasma etching by Akimoto *et al* [12].

It seems that a large dielectric plate underneath the metal wall with the slots (see figure 9(a)) is not necessary for the production of large-area non-magnetized overdense plasma. We already briefly discussed two such examples [25, 26] in section 3 above. In both cases *overdense* plasma with dimensions much larger than the skin depth δ was produced at $f = 2.45$ GHz below a metal wall with many small apertures cut into it. In both cases, however, the distances between the apertures were also of the order of δ and the apertures were almost uniformly distributed above the whole plasma region. We also confirmed experimentally that large-area plasma can be produced directly under the metal wall supporting the slots (in this case inlaid with dielectric for vacuum sealing). However we applied not many apertures, but the same local excitation with only two slots as in the normal surface-wave plasma configuration with a dielectric plate (figure 9(a)), the only difference being the absence of the dielectric plate, thus preserving one of the main advantages of the slot-excited SWP source—coupling area much smaller than the plasma area. We found that sustaining a large-area bright plasma directly under the vessel's metal wall was possible at low pressures (about 20 mTorr), while at high pressures (about 1 Torr) bright plasma was sustained only around the slots [40]. At this point it is not clear what kind of mode sustains the plasma in this case, thus strictly speaking we cannot call it SWP yet (unless it happens that the discharge is sustained by a surface wave propagating along the boundary between the underdense plasma sheet along the metal wall, which can be regarded as a dielectric, and the overdense bulk plasma). Another possibility is that the plasma is created locally around the slots and then diffuses to fill the whole chamber cross-section. This can happen because of the long diffusion length at low pressures and is consistent with the failure to observe similar behaviour at high pressures. Whatever the mode classification, the absence of the large-area dielectric plate is a great advantage, because otherwise it must withhold a huge force if used also for vacuum sealing. Thus, if one should further enlarge the slot-antenna plasma source one should either refrain from using a large-area dielectric guiding the surface wave, or should invent designs in which the large-area dielectric is *not* used for vacuum sealing, e.g. designs with local vacuum sealing only around the slot antennas.

5. Advantages of slot-excited surface-wave plasmas

In comparison to other types of high-density source, surface-wave plasmas have several advantages, especially when a slot antenna is used.

First of all, the size of the slot antenna is much smaller than the plasma diameter D. The slots launch surface waves which propagate along the plasma boundary to the

side vessel walls and are reflected there back forming a resonant eigenmode satisfying the boundary conditions. As in other resonant cavities, a singe or a few slots cut in the metal top wall are sufficient for coupling to the feeding microwave source and, thus, for producing a plasma with a diameter D much larger than the size of the coupling slot area itself. In other sources such as ICP and ECR plasma the antenna dimension is comparable to D. In this sense slot-antenna-excited plane surface-wave plasmas are superior to inductively coupled plasmas, although both sources are attractive from the viewpoint of compact and magnetic-field-free design. The local excitation allows easy up-scaling of the slot-antenna type plasma source, provided one solves the problem of the huge force which must be withstood by the dielectric window as discussed above (either by producing the plasma directly below the metal wall containing the slots, or by applying local vacuum sealing only around the slots). Thus, the most significant technical advantage of slot excitation is in the easy expandability to huge-area (>1 m^2) flat plasma.

The slot-antenna system is effective for reducing impurities such as oxygen released from the dielectric window. In ICP and helicon sources electrostatic antenna-plasma coupling gives rise to ion-induced sputtering of dielectric material near the antenna conductor. In the case of slot-antenna-excited microwave plasmas the antenna couples with the plasma electromagnetically and the wave period is too short for the ions to be accelerated so that such physical sputtering does not occur. As a consequence a much more impurity-free plasma will be produced in the slot-excited SWP.

In summary, slot excitation enables us to produce a flat, compact, clean, high-density plasma without a DC magnetic field. The working pressure covers the full range from low ($\sim$mTorr) to high ($\sim$Torr) pressures necessary for plasma processing. Further research should concentrate on optimizing the antenna structure (size, positions and number of slots) in order to achieve better mode selectivity and to become able to control the shape of the electron density profile.

6. Conclusion

The accumulated knowledge about the discharge physics of the surface-wave-sustained plasmas indicates that they are prospective candidates for the future large-area plasma processing technologies. In the present paper we tried to demonstrate that their wave structure is relatively well understood. Although density jumps may cause some problems, the stability analysis given above shows that, if the microwave launcher is properly designed and the operating point is properly chosen, stable operation can be achieved in a comfortably wide generator power range. We believe that collisionless absorption via mode conversion to an electron plasma wave is at least partially responsible for the efficient power absorption in these plasma sources. Large-area sources obtainable by simple slot excitation and clean sputtering-free high-density plasma at low gas pressures make the slot-excited SWP sources attractive for the plasma processing technologies.

References

[1] Liebermann M A and Lichtenberg A J 1994 *Principles of Plasma Discharges and Materials Processing* (New York: Wiley)
[2] Ferreira C M and Moisan M (eds) 1993 *Microwave Discharges: Fundamentals and Applications (NATO ASI series B302)* (New York: Plenum)
[3] Moisan M, Shivarova A and Trivelpiece A W 1982 *Plasma Phys.* 24 1331
[4] Ferreira C M and Moisan M 1985 *Surface Waves in Plasmas and Solids* ed S Vukovic (Singapore: World Scientific) p 113
[5] Moisan M and Zakrzewski Z 1991 *J. Phys. D: Appl. Phys.* 24 1025
[6] Zakrzewski Z and Moisan M 1995 *Plasma Sources Sci. Technol.* 4 379
[7] Moisan M, Ferreira C M, Hubert J, Margot J and Zakrzewski Z 1995 *Phenomena in Ionized Gases* ed K H Becker and W E Carr (Woodbury: AIP) p 25
[8] Zhelyazkov I and Atanassov V 1995 *Phys. Rep.* 255 79
[9] Nonaka S 1994 *Japan. J. Appl. Phys.* 33 4226
[10] Komachi K and Kobayashi S 1989 *J. Microwave Power Electromagn. Energy* 24 140
[11] Komachi K 1993 *J. Vac. Sci. Technol.* A 11 164
[12] Akimoto T, Ikawa E, Sango T, Komachi K, Katayama K and Ebata T 1994 *Japan. J. Appl. Phys.* 33 7037
[13] Fujimura S, Shinagawa K, Suzuki M and Nakamura M 1991 *J. Vac. Sci. Technol.* B 9 357
[14] Tamura H, Otsubo T, Sasaki I, Ohara K, Yamaguchi Y and Kato S 1994 *41st Natl Symp. Am. Vac. Soc.* p 191
[15] Werner F, Korzec D and Engemann J 1994 *Plasma Sources Sci. Technol.* 3 473
[16] Korzec D, Werner F, Winter R and Engemann J 1996 *Plasma Sources Sci. Technol.* 5 216
[17] Moisan M, Zakrzewski Z, Grenier R and Sauvé G 1995 *J. Microwave Power Electromagn. Energy* 30 58
[18] Ikushima T, Tochitani G and Fujita H 1995 *J. Phys. D: Appl. Phys.* 28 1851
[19] Béchu S, Boisse-Laporte C, Leprince P, Marec J 1995 *22nd Int. Conf. on Phenomena in Ionized Gases (Hoboken, 1995)* ed K H Becker, W E Carr and E E Kunhardt (Hoboken: Stevens Institute of Technology) p 149
[20] Bluem E, Béchu S, Boisse-Laporte C, Leprince P and Marec J 1995 *J. Phys. D: Appl. Phys.* 28 1529
[21] Miyano R, Shiraki Y, Fujii M, Ikezawa S, Okamoto Y, Nonaka S and Kando M 1996 *Trans. Inst. Electr. Eng. Japan* 96 31 (in Japanese)
[22] Nagatsu M, Xu G, Yamage M, Kanoh M and Sugai H 1996 *Japan. J. Appl. Phys.* 35 L341
[23] Nagatsu M, Xu G, Ghanashev I, Kanoh M and Sigai H 1996 *Proc. 13th Symp. on Plasma Processing (Tokyo)* (Tokyo: Japan Society of Applied Physics) p 9
[24] Ghanashev I, Nagatsu M and Sugai H 1997 *Japan. J. Appl. Phys.* 36 337
[25] Yoshida Y, Miyazawa T and Kazawa A 1996 *Rev. Sci. Instrum.* 68 79
[26] Hirayama M, Ohmi T 1997 *Proc. 30th Symp. on ULSI Ultra Clean Technology* (Tokyo: Ultra Clean Society) p 49

[27] Odrobina I, Kudela J and Kando M 1997 *10th Symp. on Plasma Science for Materials Abstracts (Tokyo, 1997)* (Tokyo: Japan Society for the Promotion of Science) p 47

[28] Allis W P, Buchsbaum S J and Bers A 1963 *Waves in Anisotropic Plasmas* (Cambridge, MA: MIT Press) ch 10

[29] Chen F F 1974 *Introduction to Plasma Physics* (New York: Plenum)

[30] Collin R E 1960 *Field Theory of Guided Waves* (New York: McGraw-Hill) ch 11

[31] Stenzel R L, Wong A Y and Kim H C 1974 *Phys. Rev. Lett.* 32 654

[32] Stepanov K N 1965 *Zh. Tekh. Fiz.* 35 1002 (Engl. transl. *Sov. Phys.–Tech. Phys.* 10 773)

[33] Aliev Yu M, Maximov A V, Kortshagen U, Schlüter H and Shivarova A 1995 *Phys. Rev.* E 51 69

[34] Grosse S, Georgieva-Grosse M, Ghanashev I and Schlüter M 1997 *J. Electromagn. Waves Appl.* 11 609

[35] Yoshida Y 1997 Private communication

[36] Moisan M, Baudry C, Bertrand L, Bloyet E, Gagné J M, Leprince L, Marec J, Mitchel G, Ricard A and Zakrzewski Z 1976 *4th Int. Conf. on Gas Discharges (Swansea, 1976) (IEE Conf. Publ. 143)* p 382

[37] Goubau G 1950 *J. Appl. Phys.* 21 1119

[38] Ikezawa S, Miyano R, Fujii M, Inaguma J, Shiraki Y, Kida K, Nishiwaki A, Okamoto Y, Nonaka S and Kando M 1996 *Proc. 1996 Int. Conf. on Plasma Physics (Nagoya, 1996)* ed H Sugai and T Hayashi (Nagoya: Japan Society of Plasma Science and Nuclear Fusion Research) p 1914

[39] Moisan M, Baudry C and Leprince P 1975 *IEEE Trans. Plasma Sci.* 3 55

[40] Nagatsu M, Xu G, Ghanashev I, Kanoh M and Sugai H 1997 *Plasma Sources Sci. Technol.* 6 427

[41] Ghanashev I, Xu G, Nagatsu M and Sugai H 1997 *Trans. Inst. Electr. Eng. Japan* 97 45

[42] Ghanashev I, Morita S, Nagatsu M and Sugai H 1998 *Proc. 15. Symp. on Plasma Processing (Hamamatsu, 1998)* ed S Miyake (Tokyo: Japan Society of Applied Physics) p 174

[43] Ghanashev I P and Sugai H 1997 *Proc. 3rd Int. Conf. on Reactive Plasmas (Nara, 1997)* ed K Tachibana and Y Watanabe (Tokyo: Japan Society of Applied Physics) p 375

[44] Ghanashev I, Nagatsu M, Xu G and Sugai H 1997 *Japan. J. Appl. Phys.* 36 4704

[45] Akhiezer A I and Bakai A S 1972 *Dokl. Akad. Nauk SSSR* 201 1074 (Engl. transl. *Sov. Phys.–Dokl.* 16 1065)

[46] Turner M M 1993 *Phys. Rev. Lett.* 71 1844

[47] Aliev Yu M, Kaganovich I D and Schlüter H 1997 *Phys. Plasmas* 4 2413

[48] Nagatsu M, Xu G, Ghanashev I, Kanoh M and Sugai H 1997 *Proc. 3rd Int. Conf. on Reactive Plasmas (Nara, 1997)* ed K Tachibana and Y Watanabe (Tokyo: Japan Society of Applied Physics) p 395

[49] Sugai H, Ahn T H, Ghanashev I, Goto M, Nagatsu M, Nakamura K, Suzuki K and Toyoda H 1997 *Plasma Phys. Control Fusion* 39 A445

[50] Kim H C, Stenzel R L and Wong A Y 1974 *Phys. Rev. Lett.* 33 886

[51] Ikezi H, Nishikawa K and Mima K 1974 *J. Phys. Soc. Japan* 37 766

[52] Sugai H, Maruyama M, Sato M and Takeda S 1977 *Phys. Lett.* 64A 295